Control of excitatory CNS synaptogenesis by astrocyte-secreted proteins Hevin and SPARC

Hakan Kucukdereli[a], Nicola J. Allen[b], Anthony T. Lee[a], Ava Feng[a], M. Ilcim Ozlu[a], Laura M. Conatser[a], Chandrani Chakraborty[b], Gail Workman[c], Matthew Weaver[c], E. Helene Sage[c], Ben A. Barres[b], and Cagla Eroglu[a,1]

[a]Cell Biology Department, Duke University Medical Center, Durham, NC 27710; [b]Department of Neurobiology, Stanford University School of Medicine, Stanford, CA 94305; and [c]Hope Heart Program, Benaroya Research Institute at Virginia Mason, Seattle, WA 98101

Edited* by Eric M. Shooter, Stanford University School of Medicine, Stanford, CA, and approved June 21, 2011 (received for review March 29, 2011)

Astrocytes regulate synaptic connectivity in the CNS through secreted signals. Here we identified two astrocyte-secreted proteins, hevin and SPARC, as regulators of excitatory synaptogenesis in vitro and in vivo. Hevin induces the formation of synapses between cultured rat retinal ganglion cells. SPARC is not synaptogenic, but specifically antagonizes synaptogenic function of hevin. Hevin and SPARC are expressed by astrocytes in the superior colliculus, the synaptic target of retinal ganglion cells, concurrent with the excitatory synaptogenesis. Hevin-null mice had fewer excitatory synapses; conversely, SPARC-null mice had increased synaptic connections in the superior colliculus. Furthermore, we found that hevin is required for the structural maturation of the retinocollicular synapses. These results identify hevin as a positive and SPARC as a negative regulator of synapse formation and signify that, through regulation of relative levels of hevin and SPARC, astrocytes might control the formation, maturation, and plasticity of synapses in vivo.

osteonectin | extracellular matrix | matricellular protein | synaptic cleft 1 | SPARC-Like 1

Formation of the correct type and number of synaptic connections is crucial for the proper development and function of our nervous systems. In the past decade, astrocytes have emerged as important regulators of synaptic connectivity (1, 2).

By using a purified retinal ganglion cell (RGC) culture system (3), we previously showed that astrocyte-secreted factors, including a family of ECM proteins, thrombospondins (TSPs), significantly increase the number of synapses formed between RGCs (4–6). These in vitro findings paved the way for recognition of astrocytes, and the TSPs they secrete, as important regulators of synapse formation and injury-mediated synaptic remodeling in vivo (4, 5, 7).

TSPs belong to a subclass of secreted proteins called matricellular proteins. Matricellular proteins function by modulation of cell–cell and cell–matrix interactions, and thereby regulate the adhesion state of cells (8). Astrocytes express a number of matricellular proteins in addition to TSPs, and their expression is developmentally regulated and overlaps with early postnatal periods of synaptic development in the CNS (9, 10).

In the present study we investigated whether other astrocyte-secreted matricellular proteins could modulate synapse formation. Gene expression profiling of astrocytes suggested the matricellular proteins hevin [also known as secreted protein acidic and rich in cysteine (SPARC)-like 1] and SPARC as possible candidates. Hevin and SPARC are members of the SPARC family (11). Hevin was first identified as a synaptic glycoprotein and was initially termed synaptic cleft-1, or SC1 (12). It is localized to excitatory CNS synapses (13). Astrocytes in the developing brain express high levels of hevin and SPARC mRNA, with hevin mRNA being one of the highest-level mRNAs expressed by astrocytes (10). Unlike TSP1 and TSP2, the expression of which is decreased during maturation, hevin and SPARC mRNA levels remain high in the adult (9, 14–16).

Here we investigated whether hevin and SPARC play roles in synapse formation. We found that, similarly to TSP, but unlike many other matrix and matrix-associated proteins that was previously tested (4), hevin is sufficient to induce the formation of synapses between cultured RGCs. SPARC is unable to induce synapse formation, but strongly inhibits hevin-induced synapse formation in vitro. Although both proteins promote neurite outgrowth by RGCs in culture, we show that the synaptogenic function is exclusive to hevin and that SPARC antagonizes hevin, most likely by competing for an interaction mediated by hevin's SPARC-like homology region. We also analyzed retinocollicular synapse development in WT and hevin-null mice and found that hevin is required for formation and structural maturation of excitatory synaptic boutons in the optic tectum of mice. Lack of SPARC, on the contrary, leads to enhancement of excitatory synaptogenesis in vivo. These results identify hevin and SPARC as astrocyte-secreted factors that positively and negatively regulate synapse formation and synaptic morphology. Competitive equilibrium between these two proteins could provide a molecular mechanism underlying the temporal and spatial regulation of synapse formation, maturation, and plasticity in the CNS.

Results

Hevin Is a Synaptogenic Protein Expressed by Astrocytes in Vivo and in Vitro. To confirm that astrocytes express hevin protein in vivo, we stained sagittal brain sections from a BAC transgenic *Aldh1L1*-EGFP mouse with a monoclonal antibody specific for hevin (12:155; Fig. S1*A* shows antibody characterization). In these mice, GFP is expressed in all protoplasmic astrocytes but not in any other cell type (9). Hevin staining was colocalized with GFP-labeled astrocytes, showing that astrocytes express hevin protein in vivo (Fig. 1*A*, arrows). Astroglial cultures also produced hevin protein (Fig. 1*B*).

The relative abundance of hevin in the brain and in cultured astrocytes, and its synaptic localization in the adult CNS, prompted us to test whether hevin has synaptogenic activity. To do so, we treated RGCs that had been cultured for 4 d in vitro (DIV) for an additional 6 DIV alone, or with astrocyte-conditioned medium (ACM) or in the presence of purified hevin (30 nM) or purified TSP1 (8 nM). We then immunostained these cells for pre- and postsynaptic markers such as the presynaptic active zone marker bassoon and the postsynaptic density (PSD) marker homer (Fig. 1*C*) to examine how many synapses were formed. Cells cultured alone had very few pre- or postsynaptic puncta that, for the most part, were not colocalized, indicating that these cells did not form many synapses. On the contrary, RGCs cultured in the presence of astrocytes or hevin had many pre- and postsynaptic puncta that were colocalized, which indicates that these RGCs formed synapses (Fig. 1*C*). The numbers

Author contributions: H.K., N.J.A., A.T.L., A.F., B.A.B., and C.E. designed research; H.K., N.J.A., A.T.L., A.F., M.I.O., L.M.C., C.C., G.W., and C.E. performed research; G.W., M.W., and E.H.S. contributed new reagents/analytic tools; H.K., N.J.A., A.T.L., A.F., L.M.C., and C.E. analyzed data; and H.K., E.H.S., B.A.B., and C.E. wrote the paper.

The authors declare no conflict of interest.

*This Direct Submission article had a prearranged editor.

Freely available online through the PNAS open access option.

[1]To whom correspondence should be addressed. E-mail: c.eroglu@cellbio.duke.edu.

See Author Summary on page 12983.

This article contains supporting information online at www.pnas.org/lookup/suppl/doi:10.1073/pnas.1104977108/-/DCSupplemental.

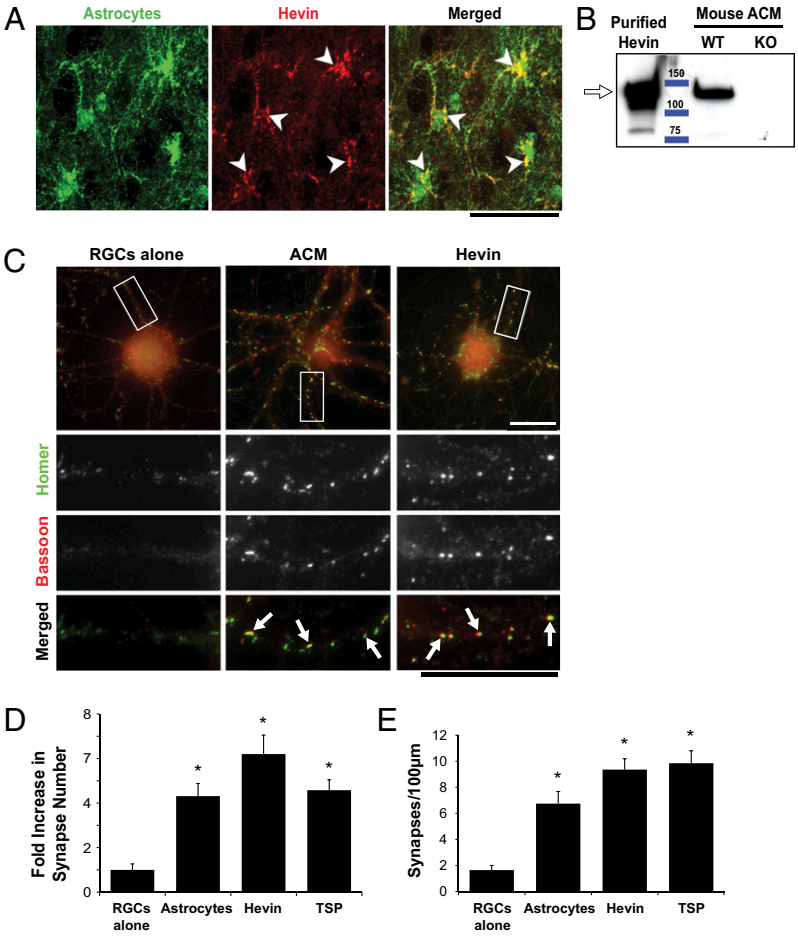

Fig. 1. Hevin is expressed by astrocytes and induces synapse formation on RGCs in culture. (*A*) A sagittal brain section from a P19 *Aldh1-L1*–EGFP transgenic mouse that expresses GFP (green) in protoplasmic astrocytes throughout the CNS was stained with a monoclonal antibody against hevin (12:155). Hevin staining (red) colocalizes (arrows) with the GFP expressing astrocytes (green). (Scale bar: 50 μm.) (*B*) Western blot analysis of astrocyte conditioned media (ACM) from WT and hevin-null mice. WT ACM shows a 130-kDa band corresponding to hevin protein (arrow), which is absent in the ACM from hevin-null (KO) mice. (*C*) Immunostaining of RGCs with presynaptic marker bassoon (red) and postsynaptic marker homer (green) showed many colocalized synaptic puncta (white arrows) in the presence of ACM or 30 nM purified recombinant hevin (*Middle*, *Right*), but few under the condition in which RGCs were cultured alone (*Left*). *Lower*: Magnified images of the white rectangles. (Scale bars: 30 μm.) (*D*) Fold increase in the number of colocalized synaptic puncta formed by RGCs in response to astrocytes (feeder layer inserts), hevin, or TSP1. Fold increase is calculated based on the number of synapses formed by RGCs cultured alone (mean synapse number for RGCs alone condition, 3.0 ± 1.0). (*E*) Graphical presentation of synaptic density changes in cultured RGCs in response to astrocytes (feeding layer inserts), hevin, or TSP1. Synaptic density indicates the number of synapses per 100 μm neurite. (*$P < 0.05$; $n = 20$ cells per condition; error bars indicate SEM).

of colocalized synaptic puncta for each condition were quantified by Puncta Analyzer, a custom-written plug-in for the National Institutes of Health (NIH) image-processing package ImageJ (described in refs. 4, 5, 17). We found that hevin, like astrocytes or TSPs, induced a significant increase in the number of synapses (as much as three- to fivefold more than that of RGCs cultured alone; Fig. 1*D*). This increase in synapse number per cell was correlated with a similar fold increase in the synaptic density per unit dendrite length (Fig. 1*E*). Correspondingly, treatment of RGCs with hevin led to a three- to fivefold increase in the colocalization of the presynaptic vesicular marker synaptotagmin and the PSD protein PSD95 (Fig. S1 *C* and *D*). Hevin concentrations higher than 13 nM induced a significant increase in synapse numbers (ranging from three to 10 fold; Fig. S1*E*).

Hevin Induces Structurally Normal and Postsynaptically Silent Synapses. To confirm the increase in synapse number after hevin treatment and to determine the ultrastructural parameters of hevin-induced synapses, we performed electron microscopy (EM) analysis of ultrathin (50 nm) sections of RGCs cultured alone, with astrocytes, or with hevin (Fig. 2*A*). We counted the number of synapses per cell (per section) by scanning the cell body and proximal dendrites within a diameter of three times that of the cell body. Consistent with the increased colocalization of pre- and postsynaptic puncta seen by immunofluorescence, the number of synapses per cell in EM was three- to fivefold higher in RGCs cultured with hevin or astrocytes than in the RGCs cultured alone (Fig. 2*B*). Synapses induced by hevin were ultrastructurally identical to the synapses induced by astrocytes, as hevin-induced synapses contained similar numbers of synaptic vesicles (total or docked) at the presynaptic terminals as observed in the astrocyte-induced synapses (Fig. 2*C*). Moreover, active zone length was essentially identical between hevin-induced and astrocyte-induced synapses (182 ± 23 nm and 202 ± 36 nm, respectively). Altogether, these data show that purified hevin is sufficient to promote formation of ultrastructurally normal excitatory synapses in vitro.

TSP family proteins are sufficient to mediate the structural formation of an excitatory synapse, but they do not promote postsynaptic function (4). To test whether hevin-induced synapses are postsynaptically active, we performed whole-cell patch-clamp recordings on RGCs cultured alone, with astrocytes, or with hevin. Hevin-induced synapses were postsynaptically silent (Fig. 2 *F*–*I* and Fig. S2). These data show that synapses formed by hevin are ultrastructurally normal and postsynaptically silent, similar to TSP-induced synapses.

Hevin Depletion from Mouse ACM Leads to a Decrease in the Number and Size of Synapses Between RGCs. To determine the relative contribution of hevin to astrocyte-induced synaptogenesis in vitro, we immunodepleted mouse astrocyte conditioned media (ACM) with polyclonal antibodies against murine hevin (Fig. 3*A*). RGCs cultured with hevin-depleted ACM formed significantly fewer synapses compared with the RGCs treated with mock-depleted ACM (~30% reduction; Fig. 3 *B* and *D*). Addition of pure hevin into hevin-depleted ACM restored the full synaptogenic potency of the depleted ACM, showing that the reduction in synapse numbers we saw in hevin-depleted ACM is caused by the loss of hevin protein (Fig. 3 *B* and *C*). In a similar experiment, when we quantified synapse numbers for RGCs treated with mock or hevin-depleted ACM, using the presynaptic vesicular marker synaptotagmin and the PSD marker PSD95, we saw a similar 30% decrease in synapse number (Fig. S3 *A* and *B*). Moreover, the synapses formed by hevin-depleted ACM were smaller in size, in

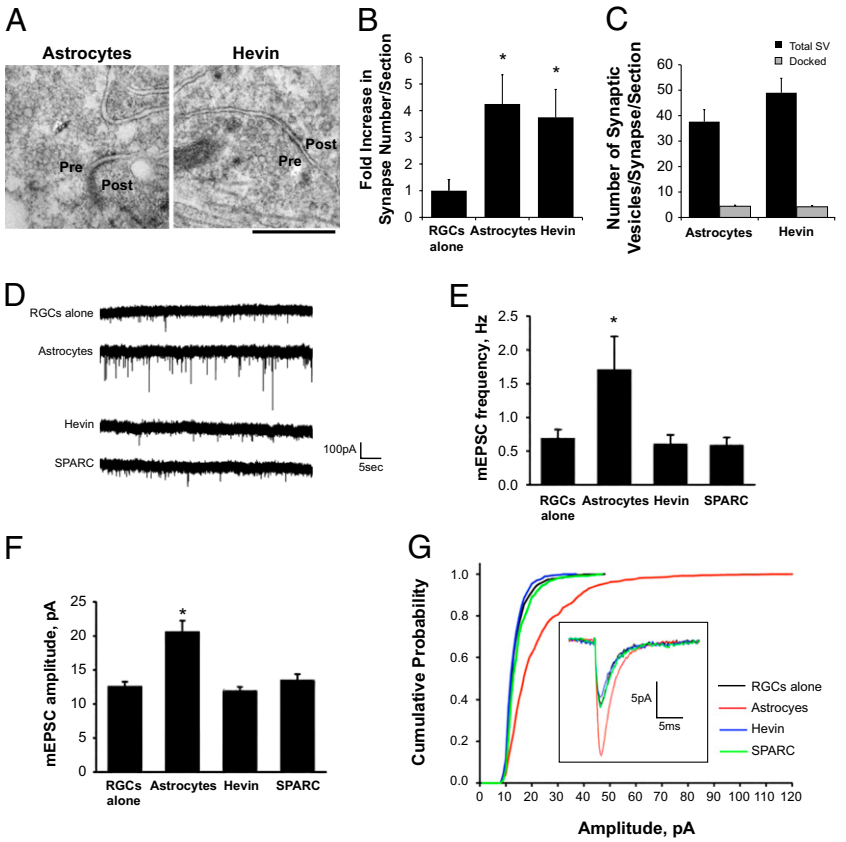

Fig. 2. Hevin-induced synapses are ultrastructurally normal but postsynaptically silent. (*A*) EM images of synapses formed between rat RGCs cultured in the presence of astrocyte feeder layer inserts (astrocytes, *Left*) or purified hevin (*Right*). Hevin-induced synapses appear ultrastructurally normal and resemble astrocyte-induced synapses. Pre, presynaptic; post, postsynaptic site. (Scale bar: 250 nm.) (*B*) Quantification of number of synapses formed onto cultured rat RGCs by EM. RGCs treated with astrocyte feeder layers or hevin formed three- to fivefold more synapses compared with RGCs cultured alone (*$P < 0.05$; $n = 8$ cells per condition, error bars indicate SEM). (*C*) Quantification of the number of synaptic vesicles per presynaptic terminal per EM section. Black bars represent the total number of synaptic vesicles per synapse per section. Gray bars represent the number of docked vesicles (within 50 nm distance of the active zone; $P > 0.05$, not significant; $n = 15$ synapses for hevin and $n = 17$ synapses for astrocyte condition; error bars indicate SEM). (*D*) Hevin-induced synapses are postsynaptically silent. Representative traces from whole-cell patch-clamp recordings of mEPSCs from RGCs cultured alone, with astrocytes, with 30 nM hevin, or with 100 nM SPARC. Only the RGCs cultured with astrocyte feeder layer inserts (i.e., astrocytes) exhibited an increase in postsynaptic events versus RGCs alone. Quantification of the frequency (*E*) and amplitude (*F*) of mEPSCs from RGCs cultured alone, with astrocytes, with 30 nM hevin, or with 100 nM SPARC (*$P < 0.01$; $n = 12$ cells per condition; error bars indicate SEM). (*G*) Cumulative probability plot of the amplitude of mEPSCs recorded from RGCs cultured alone (control), with astrocytes, with 30 nM hevin, or with 100 nM SPARC. Only the mEPSCs from RGCs cultured with astrocytes are larger than those under control conditions. *Inset*: Average waveforms of mEPSCs from RGCs cultured alone (control), with astrocytes, with 30 nM hevin, or with 100 nM SPARC ($n = 12$ cells per condition).

large part because of a decrease in the puncta size of the presynaptic vesicular marker synaptotagmin (Fig. S3 *A* and *C*).

We found that the majority of the remaining synaptogenic activity of mouse ACM after hevin depletion is a result of TSP1 and TSP2, because hevin-depleted ACM that was prepared by conditioning TSP1/2 double-null mouse astrocytes (TSP1/2KO-ACM) lacked any significant synaptogenic activity (Fig. 3*C*). Taken together, these results show that hevin accounts for part of the synaptogenic activity of the mouse ACM. In addition, lack of hevin from mouse ACM leads to a significant decrease in synaptic puncta size.

SPARC Antagonizes the Synaptogenic Function of Hevin. Rat ACM, upon TSP depletion, loses most of its synaptogenic activity, indicating that TSP1 and TSP2, which are the main isoforms expressed by astroglial cultures, are responsible for most or all of the synaptogenic effect of rat ACM (4). Because hevin did not compensate for lack of TSP in the rat ACM, we investigated whether a third factor in the ACM might be inhibitory to the synapse-forming activity of hevin.

SPARC is a homologue of hevin that is also expressed by astrocytes in vivo and is present at high levels in ACM (Fig. 4 *A* and *B*) (9, 18–20). Unlike hevin, SPARC did not promote synapse formation between RGCs in culture (Fig. 4 *C*–*F*). In addition, SPARC did not induce postsynaptic activity (Fig. 2 *D*–*G* and Fig. S2).

When we treated RGCs with a combination of hevin and SPARC (~1:3 molar ratio), the synaptogenic activity of hevin was diminished (Fig. 4 *C*–*F*). When we cocultured RGCs with TSP and SPARC (~1:3 molar ratio), SPARC did not antagonize the synaptogenic activity of TSP. The inhibitory effect of SPARC is therefore specific to hevin-induced synaptogenesis (Fig. 4 *E* and *F*).

In agreement with these observations, immunodepletion of SPARC from rat ACM resulted in a significantly higher number of synapses in comparison with mock-depleted ACM (Fig. S4 *A* and *B*). In this series of experiments, only a partial immunodepletion of SPARC was achieved as a result of the high amounts of SPARC in the rat ACM. In the SPARC-depleted condition, the RGC cell bodies and proximal dendrites were highly innervated by synaptotagmin positive axons (Fig. S4*A*). These results demonstrate that SPARC antagonizes the synaptogenic effect of hevin in the ACM. Thus, the predominant functional synaptogenic factors in rat ACM are TSPs.

SPARC is known to have neurotrophic and neurite outgrowth-promoting properties on RGCs (21, 22). Under the long-term culturing conditions used for studying synapse formation, RGC survival was not different between RGCs cultured alone or with hevin or SPARC (Fig. S4 *C* and *D*). However, both hevin and SPARC promoted neurite outgrowth and branching (Fig. S4 *E*–*G*). These results show that hevin and SPARC share the capacity to promote RGC neurite outgrowth, but only hevin is synaptogenic.

SPARC and SPARC-Like Homology Region of Hevin Antagonize Hevin's Synaptogenic Activity. Matricellular proteins such as TSPs, hevin, and SPARC mediate multiple functions through domain-specific interactions with numerous cell surface molecules (8). Hevin and SPARC have similar domain structures (Fig. 5*A*). They both have highly conserved calcium binding EF-hand regions at the C terminus, and follistatin/Kazal-like domains in the middle. Hevin has a long acidic N-terminal domain, which is unique to this protein, whereas SPARC exhibits a shorter acidic stretch at its N terminus (23).

What is the nature of the antagonistic function of SPARC? One possibility is that SPARC interacts with and sequesters hevin, and thus inhibits an interaction that is required for its activity. However, SPARC did not coimmunoprecipitate with hevin, a result indicating that these two proteins do not interact (Fig. 5*B*). Moreover, during hevin depletion from mouse ACM,

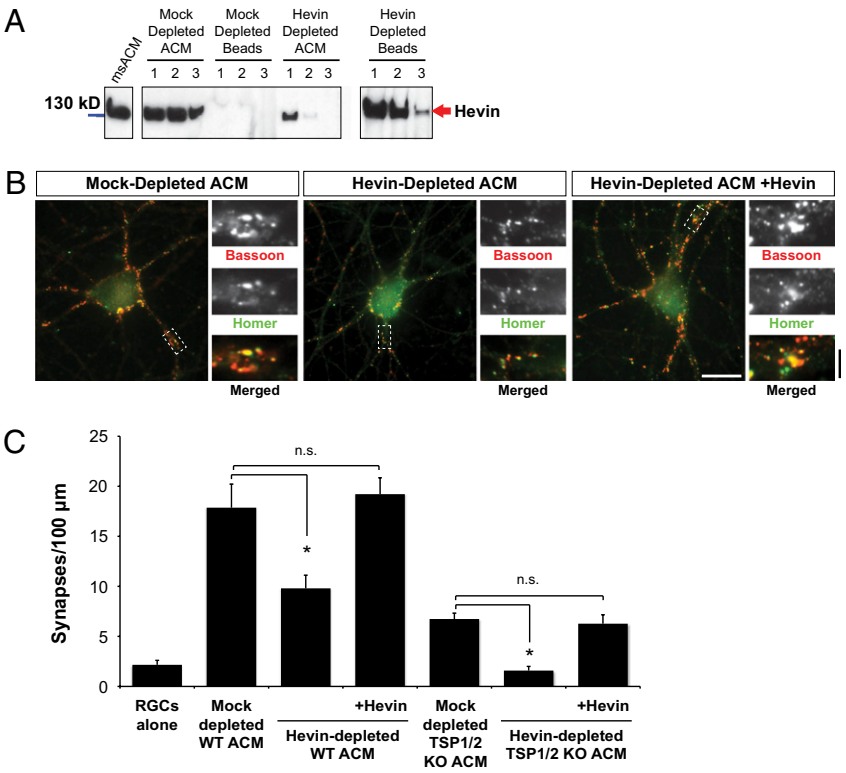

Fig. 3. Depletion of hevin from ACM reduces synapse number and synaptic size. (*A*) Hevin was immunodepleted from mouse ACM with a rabbit polyclonal antibody against mouse hevin bound to Protein A/G beads (Pierce). Mouse ACM was incubated with the antibody bound beads for three rounds (lanes marked 1, 2, and 3). Hevin was detected by Western blotting with a rat monoclonal antibody against mouse Hevin (12:155). After the third round of depletion, no hevin was detected in the ACM. Mock depletion was performed in parallel with Protein A/G beads pretreated with preimmune rabbit serum. Hevin is preserved after mock depletion. (*B*) Representative images of RGCs that were cultured with mock-depleted ACM (*Left*), hevin-depleted ACM (*Middle*), or hevin-depleted ACM supplemented with 30 nM hevin (*Right*), and stained with presynaptic marker bassoon (red) and postsynaptic marker homer (green). Magnified images corresponding to the white rectangles are presented on the right side of each panel. Colocalized puncta in merged images represent synapses (Scale bars: white, 20 µm; black, 2 µm.) (*C*) Quantification of the effects of hevin depletion from WT or TSP1/2-deficient (TSP1/2 KO) mouse ACM on synaptic density. For rescue of depletion phenotype, hevin-depleted ACM was supplemented with 30 nM hevin. Synaptic density indicates the number of synapses per 100 µm neurite (*$P < 0.05$; $n = 20$ cells per condition, n.s., not significant; error bars indicate SEM).

SPARC did not coimmunodeplete with hevin, further indicating that these proteins do not interact (Fig. S5*A*).

Because hevin and SPARC are homologous, it is possible that SPARC competitively interacts with a neuronal cell surface molecule that mediates hevin-induced synapse formation; thus, SPARC would act in a dominant-negative fashion. To test this possibility, we produced a recombinant hevin truncation construct, which contained a secretion sequence followed by amino acids 350 to 650 of the hevin molecule encompassing the SPARC homology regions within hevin [SPARC-like fragment (SLF)]. Hevin, SPARC, and SLF were expressed in HEK293 cells and were purified from conditioned media (Fig. S5*B*). RGCs were treated with 30 nM hevin in the presence of increasing molar ratios of purified SPARC or SLF (Fig. 5 *C* and *D*). We found that SLF mimicked the antagonistic effect of SPARC with a similar dose–response curve and blocked hevin-induced synapse formation at a molar ratio of 1:2 and greater (Fig. 5 *C* and *D*). Neither SPARC nor SLF was synaptogenic at any of the concentrations we used (Fig. S5 *C* and *D*). SLF promoted neurite outgrowth and branching similar to hevin and SPARC (Fig. S4 *E*–*G*). These results strongly indicate that SPARC blocks hevin-induced synapse formation by competition with an interaction that is established by the SPARC-like homology region of hevin. In addition, these results also show that the neurite outgrowth promoting function of hevin is mapped to its SPARC homology region.

Hevin and SPARC Control Formation of Retinocollicular Synapses in Vivo. To test whether hevin and SPARC regulate synapse formation in vivo, we focused on the optic tectum of mice, the superior colliculus (SC), where RGC axons form excitatory synaptic contacts. RGC axons reach their targets at the SC before birth, but the vast majority of synaptic contacts are formed in the SC during the second and third week of postnatal development (24, 25). Western blotting analysis of SC lysates derived from mice at various postnatal time points with antibodies specific for hevin or SPARC (characterized in Fig. S6 *A* and *B*, respectively) showed that hevin gradually increases during the first two postnatal weeks, reaching a peak at approximately postnatal day (P) 15 to P25 that correlates with the peak of the synaptogenic period in the SC, and remains high throughout adulthood (Fig. 6 *A* and *B*). SPARC expression also peaks at P15 to P25 (Fig. 6 *A* and *B*; bars represent an average of four different blots using SC lysates from four different animals for each age).

To visualize hevin and SPARC expression in the SC, we immunostained for these proteins in sagittal mouse brain sections at P5, before the synaptogenic period starts; at P15, the midpoint of the synaptogenic period; and at P25, after most of the synapses are formed and mature (Fig. 6 *C* and *D*). Similar to the results from Western blotting, at P5, we observed little hevin staining, located mostly in the parenchyma of the SC. The expression pattern indicated that hevin was localized to the cortical part of the SC immediately underneath the pial surface (Fig. 6*C*, *Left*). At P15 and P25, we observed a strong staining for hevin in the SC. The pattern of staining looked astrocytic in origin (Fig. 1*A* shows localization of hevin staining in EGFP-labeled astrocytes) and was localized to the ECM and to the astrocytes (Fig. 6*C*, *Middle*, white arrows). In agreement with previous studies that showed that hevin is localized to excitatory synapses and perisynaptic astrocytic processes (12, 13), in the SC, extracellular punctate hevin signal often colocalized with pre- and postsynaptic markers specific for excitatory RGC synaptic terminals (Fig. 6*D*).

At P5, punctate staining for SPARC was concentrated on radial processes (Fig. 6*E*, *Left*, white arrows), which were determined to be radial glia by their costaining with anti-nestin antibody at P1 and P5 (Fig. S6*C*). Like Hevin at P15 and P25, SPARC appeared astrocytic (Fig. 6*E Middle*; Fig. 3*A* shows localization of SPARC staining in EGFP-labeled astrocytes). This astrocytic SPARC and hevin staining was colocalized (Fig. 6*F*). Comparative Western blot analysis of SC lysates from P15 mice against pure hevin or SPARC proteins estimated an approximately 6:1 (wt/wt) ratio between hevin and SPARC proteins, which corresponds to a molar ratio of approximately 3:1 (hevin: SPARC; Fig. S6 *C* and *D*). These data show that hevin is highly expressed in the SC during the synaptogenic period, and its expression is maintained into adulthood. In the developing SC, astrocytes express lower amounts of SPARC than hevin.

To test directly whether hevin and SPARC are involved in the formation of synapses by RGC axons onto their SC targets, we analyzed synapse numbers at P14 in hevin-null (Hevin-KO) or

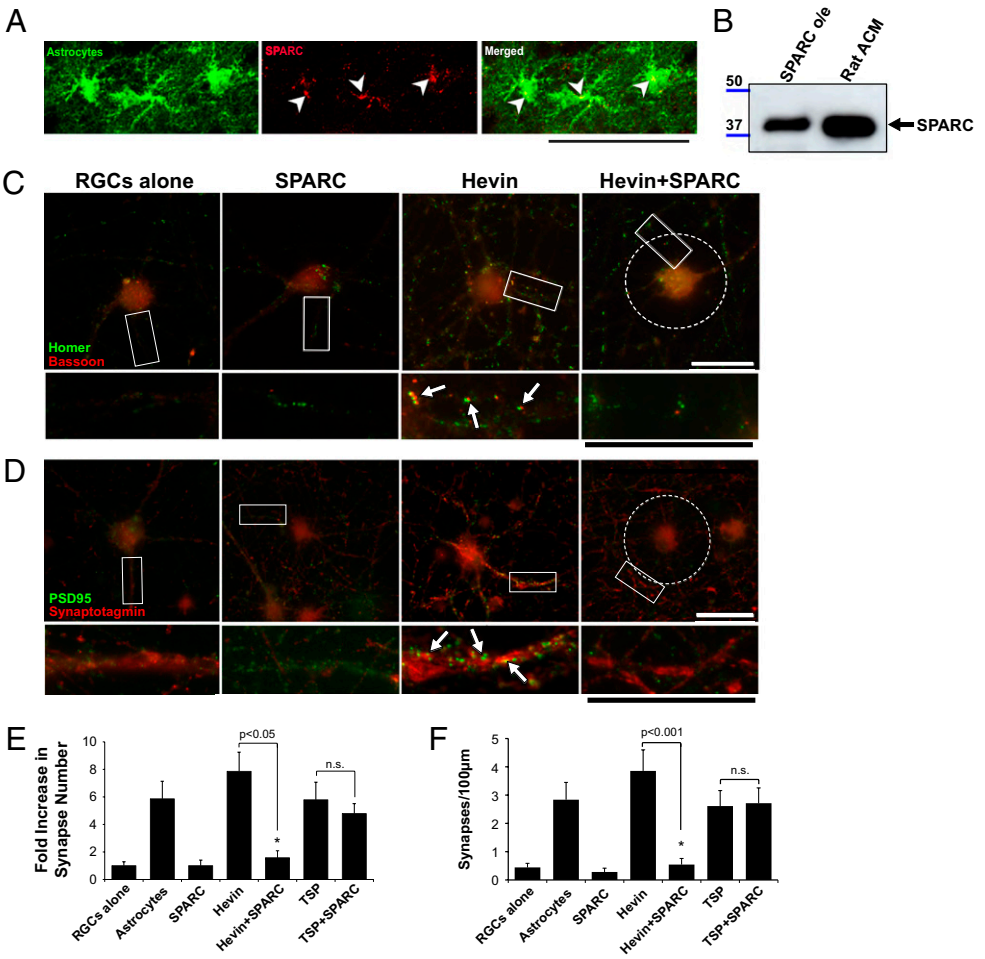

Fig. 4. SPARC antagonizes the synaptogenic activity of hevin. (*A*) A sagittal brain section from a P19 *Aldh1-L1*–EGFP transgenic mouse that expresses GFP (green) in protoplasmic astrocytes throughout the CNS was stained with goat anti-SPARC antibody (R&D Systems). SPARC staining (red) colocalizes (arrowheads) with the GFP expressing astrocytes (green). (Scale bar: 50 μm.) (*B*) Western blot analysis of rat ACM shows a 43-kDa band corresponding to SPARC protein (black arrow). SPARC o/e, HEK293 cell culture supernatant from cells expressing SPARC. (*C* and *D*) Representative images of RGCs that were cultured alone or treated with SPARC (100 nM), hevin (30 nM), or both (30 nM hevin, 100 nM SPARC) and stained with antibodies against presynaptic [red; (*C*) bassoon or (*D*) synaptotagmin] and postsynaptic [green; (*C*) homer or (*D*) PSD95] markers. RGCs cultured alone or treated with SPARC (100 nM) did not have many colocalized synaptic puncta, whereas hevin induced formation of synapses (white arrows). Addition of hevin and SPARC at the same time led to the complete loss of the synaptogenic activity of hevin (*Right*), although pre- and postsynaptic clusters were still visible (see lower panels). In this condition, presynaptic synaptotagmin clusters were excluded from the cell body and proximal dendrites (white circle). (Scale bars: 30 μm.) Quantification of the fold changes in colocalized synaptic puncta number per cell (*E*) and synaptic density (*F*) for RGCs cultured alone, with astrocyte feeder layers, hevin (30 nM), SPARC (100 nM), hevin plus SPARC (30 nM and 100 nM, respectively), TSP1 (8 nM), and TSP1 plus SPARC (8 nM and 100 nM, respectively). Fold increase is calculated based on the number of synapses formed by RGCs cultured alone (mean synapse number for RGCs alone condition, 0.933 ± 0.27; $*P < 0.05$; $n = 20$ cells per condition; n.s., not significant; error bars indicate SEM).

SPARC-null (SPARC-KO) mice at the superficial layer of the SC and compared them versus those present in WT mice of corresponding background. To do so, we stained sagittal SC sections with an antibody against a presynaptic marker that is specific for RGC synaptic terminals, the vesicular glutamate transporter 2 (VGlut2), and a marker for glutamatergic postsynaptic specializations, PSD95, and quantified the number of colocalized synaptic puncta (details of the assay can be found in *SI Materials and Methods* and Fig. S7 *A* and *B*). At P14, the number of synapses was 35% less in hevin-null brains than in WT brains. Conversely, at P14, SPARC-null mice had around a 70% increase in the number of VGlut2/PSD95-positive synapses at the SC in comparison with WT mice (Fig. 7 *A* and *B*). These results show that hevin and SPARC, respectively, are positive and negative regulators of excitatory synapse formation in vivo.

To determine whether the decreased synapse number we observed at P14 in hevin-null mice could be explained by changes in dendritic outgrowth and morphology, Golgi–Cox-stained sections from WT and Hevin-KO mice were analyzed (Fig. 7*C*). We focused on two types of RGC target neurons (WFII class and stellate class; Fig. 7*D*) (26, 27). There were no significant changes in the dendritic outgrowth, perimeter, and complexity between WT and Hevin-KO animals (Fig. 7 *E*–*G*). The decrease in synapse number was also not a result of lack of RGC axonal innervations at the SC of the KO mice, because when we injected fluorescent dye conjugated to cholera toxin-β into the left eyes of P3 WT and KO mice and analyzed RGC axonal innervations at P4—an age when the axonal innervation of SC by RGC axons is complete—the area of axonal labeling in KOs was essentially identical to that of WT (Fig. S7 *C* and *D*). These data show that the lower synaptic density observed in P14 Hevin-KO mice is not a result of defects in dendritic outgrowth or lack of axonal innervation, but of a specific defect in synapse formation.

Hevin Controls Size of Excitatory Synapses in the SC. RGC axonal terminals in SC are characterized by large presynaptic boutons enriched in synaptic vesicles (25, 28). These presynaptic boutons can be visualized by staining with VGlut2 (Figs. 7*A* and 8*A*, WT, arrows). In Hevin-KO mice, these boutons were noticeably smaller in size (Figs. 7*A* and 8*A*, dashed circles). Quantification of the area of colocalized synaptic puncta revealed that synapses made by Hevin-KO mice were significantly smaller in size than in WT at P14, and this difference persisted into P25 (Fig. 8*B*). These results indicated that, in addition to lower synaptic density, excitatory synapses at RGC terminals in Hevin-KO mice might have morphological defects.

For a detailed analysis of synaptic structure in Hevin-KO mice, we analyzed the ultrastructure of the asymmetric (i.e., glutamatergic) synapses within the superficial gray layer, stratum griseum superficiale (SGS), of the SC by EM (Fig. 8*C*). The vast majority of glutamatergic inputs in SGS are of RGC origin (29). Morphometric analysis of asymmetric synapses at the SGS of P25 mice ($n = 3$ animals per genotype; WT, 431 asymmetric synapses analyzed; KO, 289 asymmetric synapses analyzed) showed that, despite the similarity in PSD length in both WT and Hevin-KO animals, all the other synaptic parameters were significantly

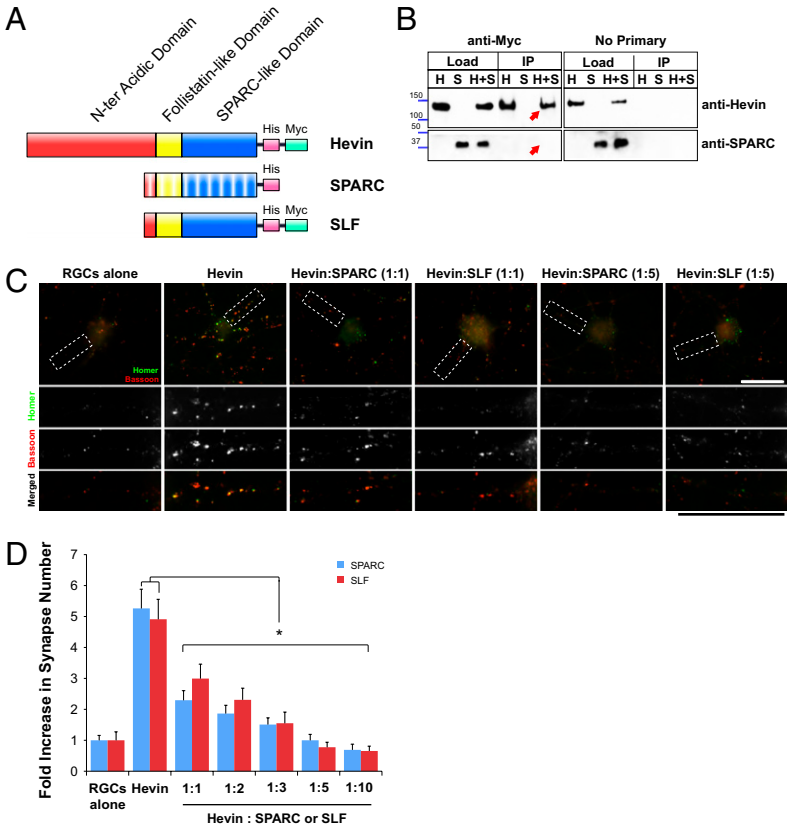

Fig. 5. SPARC and C-terminal SLF of hevin antagonize hevin-induced synapse formation in a dose-dependent manner. (*A*) Schematic representation of domain structure of hevin, SPARC, and hevin truncation construct SLF. SPARC and hevin are composed of C-terminal SPARC-like (blue) and follistatin-like domains (yellow) and N-terminal acidic domains (red). SPARC and hevin are 60% identical at their C-terminal regions; however, they have low homology at the N terminus. The recombinant proteins used in this study contained tags (6-histidine tag and/or myc tag) for purification and immunoprecipitation. (*B*) Hevin does not interact with SPARC. Purified hevin was immunoprecipitated with an anti-myc tag antibody bound to Protein A/G beads (Pierce; *Left*). SPARC did not coimmunoprecipitate with hevin. Hevin was detected with goat anti-hevin polyclonal antibodies (*Upper*), and SPARC was detected with goat anti-SPARC polyclonal antibodies (R&D Systems; *Lower*). The experiment was repeated without anti-myc tag antibody (no primary; *Right*) as a negative control. *H*, purified hevin; *S*, purified SPARC; *H+S*, hevin and SPARC together. (*C*) Representative images of RGCs that were cultured alone or with hevin or with hevin plus SPARC or Hevin plus SLF (1:1 and 1:5 molar ratios), stained with the presynaptic marker bassoon (red) and the postsynaptic marker homer (green). Colocalized puncta in merged images represent synapses. (Scale bars: 30 μm.) (*D*) Quantification of the fold changes in colocalized synaptic puncta number per cell for RGCs cultured alone, with hevin (30 nM), and with hevin plus increasing concentrations of SPARC or SLF. Fold increase is calculated based on the number of synapses formed by RGCs cultured alone [mean synapse numbers for RGCs alone, 3.05 ± 0.48 (SPARC set) and 2.58 ± 0.70 (SLF set); $*P < 0.05$; $n = 20$ cells per condition; error bars indicate SEM).

different in Hevin-KO compared with WT mice (Fig. 8*D* and Tables S1 and S2). In Hevin-KO mice, asymmetric synapses had thinner PSDs, larger synaptic cleft distances, and smaller presynaptic terminals (Fig. 8*D*). The number of synaptic vesicles, both total pool and docked, was significantly less in Hevin-KO mice (Fig. 8 *C* and *D* and Tables S1 and S2). Furthermore, we found that the number of asymmetric synapses per unit area (i.e., synaptic density) was significantly less in Hevin-KO mice compared with WT animals (Fig. 8*E* and Tables S1 and S2). The density of symmetric (i.e., inhibitory) synapses did not change significantly between genotypes (Fig. 8*E* and Tables S1 and S2). There was also a significant difference in the number of large excitatory presynaptic boutons that had "multiple" release sites between WT and Hevin-KO mice (Fig. 8*E*). These results show that hevin is an important regulator of the formation and morphology of excitatory synapses in the developing SC.

Discussion

Astrocytes Control Structural Establishment of Excitatory CNS Synapses Through the Matricellular Proteins Hevin, SPARC, and TSP. Here we identified hevin, a known component of the synaptic cleft in the adult CNS, as an astrocyte-secreted factor that induces ultrastructurally normal synapses that are postsynaptically silent. In addition to its effects on synaptogenesis, hevin also regulates synapse size. Unlike TSPs 1 and 2 that are primarily expressed in the developing brain but are subsequently down-regulated, hevin continues to be expressed at high levels by astrocytes in the adult brain. Thus, in addition to promotion of synapse formation in the developing brain, hevin might participate in synaptic maturation and maintenance.

Here we also found that, besides stimulating synapse formation, astrocytes inhibit synaptogenesis by releasing an anti-synaptogenic protein, SPARC. In vitro astrocytes produce high levels of SPARC that block the majority of the synaptogenic function of hevin in the ACM, making TSPs 1 and 2 the primary synaptogenic factors emanating from rat astrocytes in culture. When RGCs were treated concomitantly with hevin and its antagonist SPARC, the pre- and postsynaptic markers were clustered, but these clusters were not colocalized, reminiscent of the phenotype previously observed by Christopherson and colleagues after TSP depletion from rat ACM (4).

SPARC blocked hevin-induced synapse formation but did not affect the capacity of TSP to induce synaptogenesis. TSP family proteins mediate their synaptogenic function through an interaction with a neuronal cell surface molecule, calcium channel subunit α2δ-1 (5). Calcium channel subunit α2δ-1 is also the receptor for the antiepileptic, antianalgesic drug gabapentin. We recently showed that gabapentin is an inhibitor of TSP-induced synapse formation (5). These results indicate that the structural assembly of excitatory synapses can be mediated via different astrocytic proteins such as hevin and TSP, and proteins such as SPARC or small molecules such as gabapentin can negatively regulate each synaptogenic signaling pathway. It is possible that TSPs play a primary role in the induction of synapses, whereas hevin could also function in the morphological maturation and continued maintenance of synapses. This possibility is consistent with their time courses of expression in vivo and the defects in synaptic morphology we observed in hevin-null mice.

An interesting question arising from these findings is whether SPARC can also dissolve preexisting synapses or reverse them into an immature state and thus contribute to plasticity of circuits. Although there is no direct evidence that SPARC expression changes in adult-specific types of synaptic plasticity, a recent study showed that neuronal activity can regulate SPARC expression by astrocytes in vitro and SPARC-null mice have defects in synaptic plasticity (30). This study proposed that SPARC inhibits glutamate responsiveness of synapses by decreasing surface levels of AMPA glutamate receptors (30). Because hevin induced only silent synapses, this effect of SPARC cannot be directly attributed to antagonism of hevin action. However, as hevin is required for recruitment of pre- and postsynaptic machinery to the synapses, the hevin–SPARC antagonism may in-

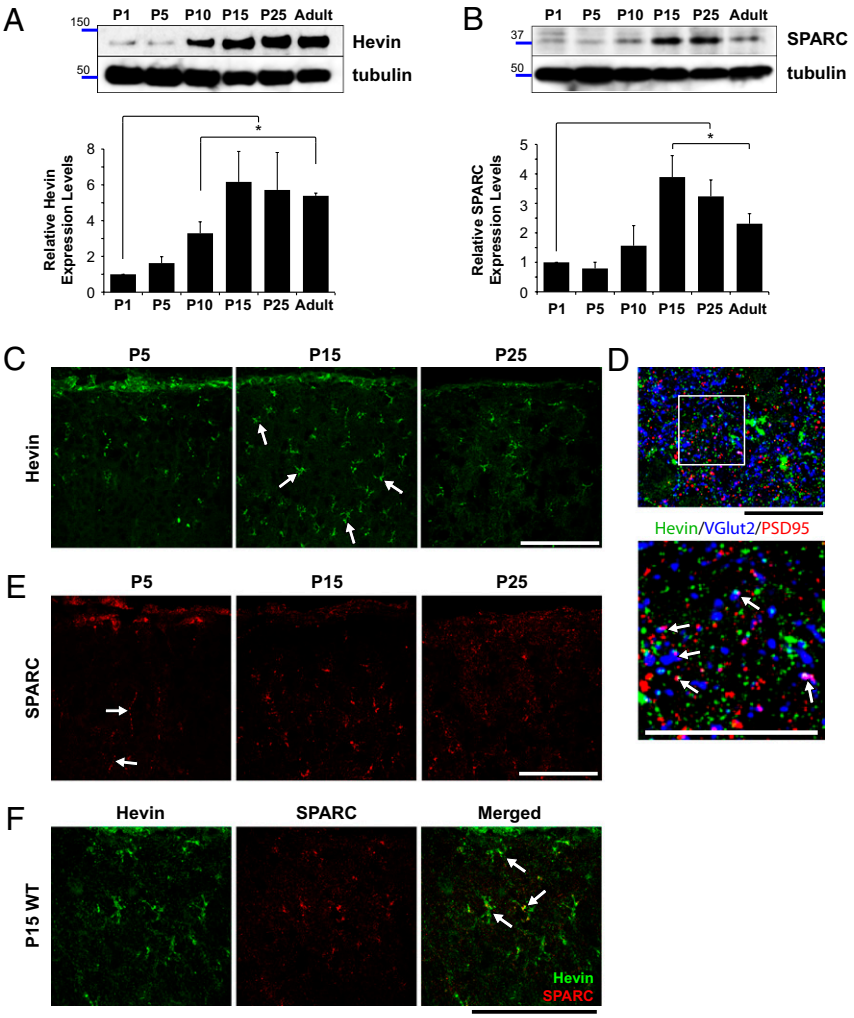

Fig. 6. Expression of hevin and SPARC is developmentally regulated at the SC. (*A*) *Upper*: Representative Western blot analysis of hevin in SC lysates from P1, P5, P10, P15, P25, and adult mice. *Lower:* Tubulin as loading control. Graph shows quantification of relative expression levels of hevin protein in SC lysates. The expression levels were quantified first by normalization of the hevin signal to the tubulin signal, and subsequently by calculation of the ratio with respect to mean hevin signal level at P1 ($n = 4$ animals per age, four separate Western blots; $^*P < 0.05$; error bars indicate SEM; Fig. S6 shows antibody characterization). (*B*) *Upper*: Representative Western blot of SPARC protein expression in SC lysates from P1, P5, P10, P15, P25, and adult mice. *Lower:* Tubulin as loading control. Graph shows quantification of relative expression levels of SPARC protein in SC lysates. The expression levels were quantified first by normalization of the SPARC signal to the tubulin signal, and subsequently by calculation of the ratio with respect to mean SPARC signal level at P1 ($n = 4$ animals per age, four separate Western blots; $^*P < 0.05$; error bars indicate SEM; Fig. S6 shows antibody characterization). (*C*) Sagittal mouse brain sections from P5, P15, and P25 mice were stained for hevin with goat anti-hevin polyclonal antibodies (green; R&D Systems). Images are taken from SC. (Scale bars: 100 μm.) (*D*) High-magnification images from SC that was stained for hevin (12:155; green); a presynaptic marker that is specific for RGC axonal terminals, VGlut2 (blue; Synaptic Systems); and the postsynaptic marker that is specific for excitatory synapses, PSD95 (red; Zymed). (Scale bars: 25 μm.) (*E*) Sagittal mouse brain sections from P5, P15, and P25 mice were stained for SPARC with goat anti-SPARC polyclonal antibody (red; R&D Systems). Images are taken from SC. (Scale bars: 100 μm.) (*F*) Hevin and SPARC proteins are colocalized at P15 (SC). *Upper:* Sagittal P15 mouse brain sections were stained for hevin and SPARC with rat anti-hevin (12:155) and goat anti-SPARC antibodies (R&D Systems). *Lower:* Hevin and SPARC colocalize in the P15 mouse SC (arrows). (Scale bar: 100 μm.)

directly regulate AMPA receptor recruitment to the synapses in vivo. Future studies investigating the role of hevin and SPARC in adult forms of plasticity will be necessary to understand the full extent of the functions of these molecules in the CNS.

Hevin Regulates Timing of Formation and Morphological Maturation of Excitatory Synapses. During development, RGC axons reach their SC targets by embryonic day 16, but form very few synapses until the end of the first postnatal week (24, 25). In the course of the second and third week of development, there is a synaptogenic period in the SC. In agreement with a role in synapse formation, hevin and SPARC protein levels are low at birth and are at their highest concurrently with synaptogenesis. Our analysis of the P14 hevin and SPARC-null mice showed that the lack of hevin leads to a reduced excitatory synaptic density, whereas SPARC-null mice display exuberant synapse formation at the SC. These in vivo findings show that hevin stimulates excitatory synapse formation, and that this function of hevin is negatively regulated by SPARC during development.

After the end of the third postnatal week and into adulthood, retinocollicular synapses mature and become bouton-like structures with large presynaptic terminals containing many synaptic vesicles (25). The classical EM studies on the developing rodent brain showed that, as the excitatory synapses mature, the postsynaptic densities become thicker (31). Our results show that lack of hevin in the SC results in a substantial decrease in the size of the presynaptic boutons and the number of synaptic vesicles. In addition, lack of hevin leads to decreased PSD thickness and significantly larger synaptic clefts. These striking defects in synaptic morphology indicate that hevin not only participates in the formation of excitatory synapses but also in their structural maturation. Hevin is also enriched in the perisynaptic astrocytic processes (13). Astrocyte ensheathment of excitatory synapses is thought to be critical for the stability and maturation of the synapse (2). Thus, in the future, it would be interesting to investigate how lack of hevin affects astrocyte–synapse interactions.

How Do Hevin and SPARC Control Synapse Formation? Hevin has been studied in systems other than the CNS as a modulator of the adhesion state of cells (23). The function of hevin in synapse formation might depend on its regulation of axon–dendrite adhesion. For example, hevin might act by clustering transsynaptic adhesion molecules and thereby promote formation of a synaptic adhesion and facilitate the recruitment of pre and postsynaptic machinery at new synapses. Alternatively, hevin might organize the structural ECM components surrounding the cell body and proximal dendrites such that the axons can establish an attachment. It is also possible that, like TSPs, hevin acts through a specific interaction with a cell surface receptor that regulates a synaptogenic pathway. Interaction partners for hevin are not well characterized; however, SPARC is known to interact with several cell surface and secreted molecules. For example, SPARC binds to integrins containing the β-1 subunit (32) and activates integrin-linked kinase pathways (33). SPARC also binds to and sequesters growth factors such as VEGF and thereby regulates growth factor–receptor interactions (34, 35). In addition,

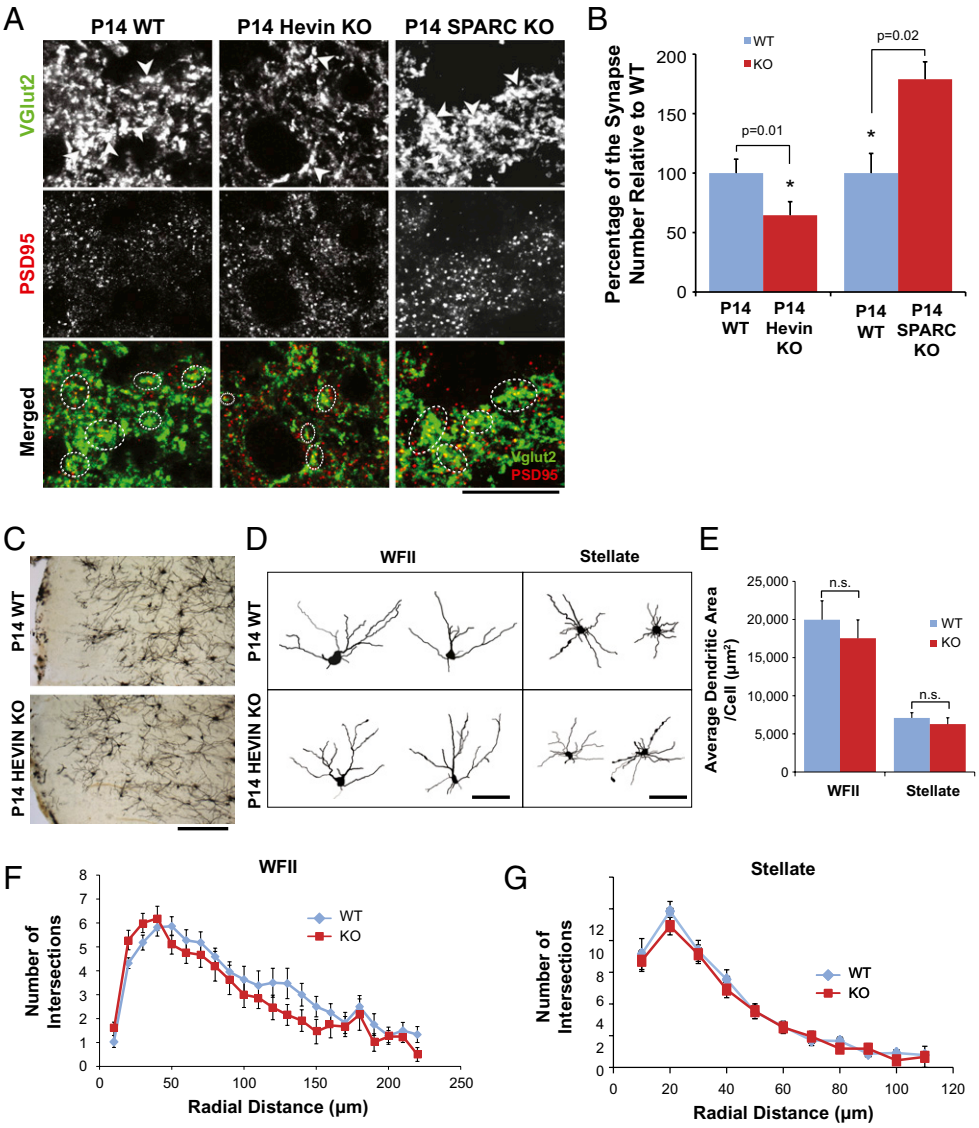

Fig. 7. Hevin-null and SPARC-null mice display defects in retinocollicular synaptogenesis. (*A*) High-magnification images from synaptic staining of SC in WT, hevin-null (Hevin KO), and SPARC-null (SPARC KO) mice at P14. *Top:* Presynaptic marker VGlut2 staining. Arrowheads point to some of the VGlut2-positive presynaptic boutons made by RGC axons. *Middle*: Postsynaptic marker PSD95 staining. *Bottom:* Merged images of presynaptic VGlut2 (green) and postsynaptic PSD95 (red) immunostaining. Dashed circles outline some of the synapses. (Scale bar: 20 μm.) (*B*) Percent change in the number of retinocollicular synapses at P14 in Hevin-KO and SPARC-KO mice relative to WT mice. Synapses were quantified as the colocalization of the presynaptic marker VGlut2 and the postsynaptic marker PSD95 (n = 4 animals per genotype per age; 15 images per animal per age were analyzed; *P = 0.01; error bars indicate SEM; Fig. S7 provides further details). (*C*) Representative images of Golgi–Cox staining of SC regions in WT and Hevin-KO mouse brains at P14. (Scale bar:100 μm.) (*D*) Representative tracings for two major RGC target neuron types, WFII and stellate, from the WT and Hevin-KO mouse SC. (Scale bar: 100 μm.) (*E*) Convex hull analysis of WT and Hevin-KO WFII and stellate neurons showed no significant differences in dendritic area between genotypes (n = 22 for each neuron type; error bars indicate SEM). Sholl analysis of WT and Hevin-KO WFII (*F*) and stellate (*G*) neurons revealed no significant differences in dendritic complexity (n = 22 for each neuron type; error bars indicate SEM).

SPARC has profound effects on ECM assembly through its specific interaction with collagen (36). Future studies to identify neuronal hevin and SPARC interactors and their role in synapse formation will be necessary to address how SPARC and hevin regulate synapse formation. Our finding that the SLF of hevin can mimic SPARC and antagonize the synaptogenic function of hevin provides evidence that SPARC competes for a common binding partner with hevin. It is likely that hevin, with its unique N-terminal acidic region, establishes a second interaction, which is crucial for its synaptogenic activity. This would explain how SPARC and SLF could inhibit hevin-induced synapse formation by blocking the binding of hevin to both sites simultaneously. Future structure–function analysis of hevin and SPARC will be helpful for the identification of candidate neuronal receptors and signaling mechanisms involved in excitatory synapse formation.

Our result that the SLF portion of hevin can antagonize its synaptogenic function also has relevance in vivo. Recently analysis of hevin in the adult brain revealed the presence of a proteolytic cleavage product of hevin—an SLF exactly the same length as the SLF fragment we used in this study—that is generated by the proteinase ADAMTS4 (37). ADAMTS4 expression and hevin proteolysis could be controlled in vivo by an activity-dependent mechanism that would provide an additional regulatory control on the synapse organizing activity of hevin.

In addition to the proteolytic processing of hevin, activity-dependent changes in the production of hevin and SPARC might occur and would contribute to synaptic plasticity throughout development and in the adult. For example, expression of both these proteins by astrocytes could be regulated by experience-dependent mechanisms. In agreement with this possibility, the period between P15 and P25, when hevin and SPARC increase in the SC, corresponds to a significant developmental period in the visual system, in which the opening of the eyes (circa P12–P14) leads to activity-dependent changes that affect the formation, maturation, and elimination of synapses (38). Moreover, a recent study on the molecular mechanisms of resilience—the ability of individuals to escape the deleterious effects of stress—identified the transcription factor DeltaFosB to be an essential regulator of this process. Hevin (i.e., SC1) was found to be a downstream target of this transcription factor (39). Injection of viruses that express hevin into mouse brain reversed the effects of social defeat, promoted resilience, and showed antidepressant-like action (39). Our results identifying a function for hevin in CNS synapse formation, together with the findings showing a role for hevin in the molecular pathway underlying resilience and antidepressant action, indicate that hevin is an important protein regulating nervous system function and behavior. The expression of SPARC and hevin are also altered after injury and in diseases

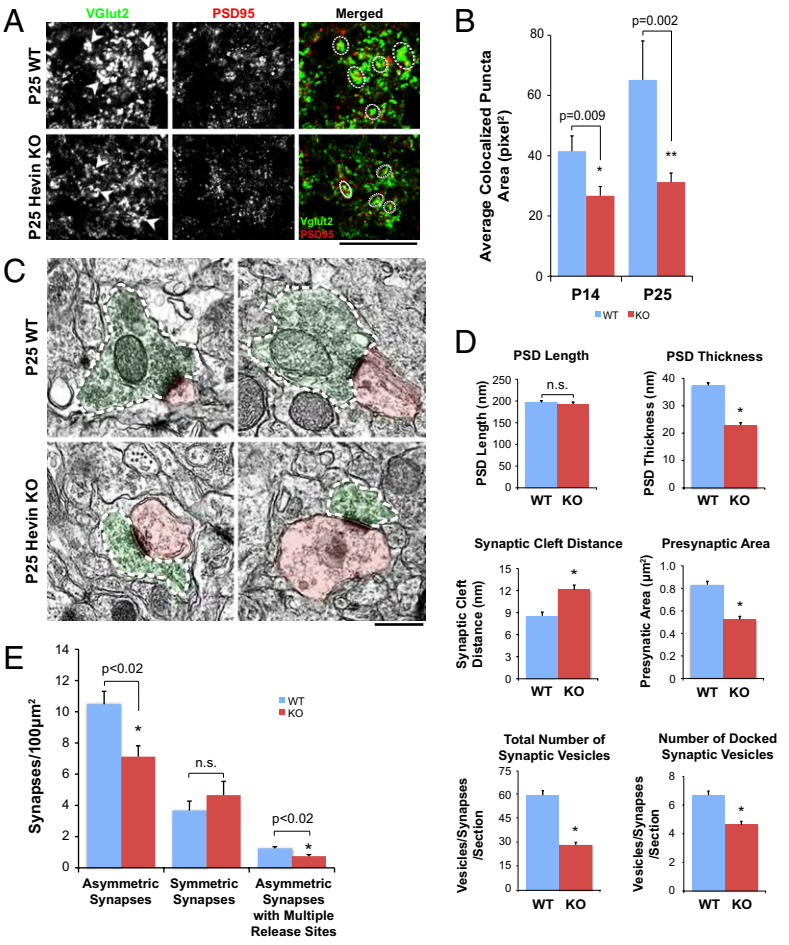

Fig. 8. *Hevin*-null mice (KO) display defects in the morphology of retinocollicular synapses. (*A*) High-magnification images from synaptic staining of SC in WT (*Upper*) and hevin KO (*Lower*) mice at P25. *Left*: Presynaptic marker VGlut2 staining. Arrowheads point to some of the VGlut2-positive presynaptic boutons made by RGC axons. *Middle:* Postsynaptic marker PSD95 staining. *Right*: Merged images of presynaptic VGlut2 (green) and postsynaptic PSD95 (red) immunostaining. Dashed circles outline some of the synapses. (Scale bar: 20 μm.) (*B*) Quantification of average colocalized synaptic puncta area in WT versus hevin-KO mice at P14 and P25. (n = 4 animals per genotype per age; 15 images per animal) Average synaptic area (i.e., area of colocalized puncta) was significantly smaller in KO animals at ages P14 and P25 (*$P < 0.01$ and **$P = 0.02$; error bars indicate SEM). (*C*) Representative EM images of synapses from WT (*Upper*) and hevin-KO mouse SCs at P25. Green represents presynaptic site and red indicates postsynaptic site. White dashed lines outline presynaptic boutons. (Scale bar: 500 nm.) (*D*) Quantification of morphological synaptic parameters of the synapses of WT and hevin-KO mouse SCs: PSD length, PSD thickness, synaptic cleft distance, presynaptic bouton area, total number of synaptic vesicles, and number of docked synaptic vesicles at P25. (*$P <$ 0.0001; n.s., not significant; error bars indicate SEM). (*E*) Quantification of synaptic density of asymmetric and symmetric synapses, and asymmetric synapses with multiple release sites, in WT and KO mouse SCs at P25. EM analysis showed that Hevin-null SC have 27% less asymmetric synaptic density compared with WT. In addition, density of asymmetric synapses with multiple presynaptic release sites is 34% less in hevin-null SC than WT. (*$P < 0.02$; n.s., not significant; error bars indicate SEM).

such as epilepsy and gliomas (14, 40–42). These pathological conditions might shift the fine balance between hevin and SPARC, which could contribute to the synaptic dysfunction associated with these diseases.

In conclusion, our results identify hevin as a positive and SPARC as a negative regulator of synapse formation and signify that, through regulation of relative levels of hevin and SPARC, astrocytes might control the formation, maturation, and plasticity of synapses in vivo.

Materials and Methods

Purification and Primary Culture of RGCs and Astrocytes. RGCs were purified by sequential immunopanning to greater than 99.5% purity from P5 to P7 Sprague–Dawley rats (Charles River) and cultured in serum-free medium containing BDNF, ciliary neurotrophic factor (CNTF), and forskolin on laminin-coated coverslips as previously described (3, 4, 6). Cortical astrocyte inserts and ACM were prepared as described (4). RGCs were cultured for 3 to 4 d to allow robust process outgrowth and subsequently cultured with astrocyte inserts, ACM, hevin, SPARC, SLF, or TSP for an additional 6 d. Detailed methods can be found in *SI Materials and Methods*.

Recombinant Proteins and DNA Constructs. Full-length hevin cDNA, as well as its truncation construct SLF, were cloned into pAPtag5 vector (GeneHunter) between SfiI and XhoI sites. Hevin constructs were expressed by HEK293 cells, which were transfected using Lipofectamine 2000 (Invitrogen) according to the manufacturer's instructions. The secreted recombinant proteins were purified from conditioned culture media by Ni-chelating chromatography by using Ni-NTA resin (Qiagen) according to the manufacturer's instructions. Purified human platelet TSP1 was obtained from Haematologic Technologies. Purified full-length SPARC was prepared as described previously (43).

Quantification of Synapses by Immunohistochemistry. For synapse quantification of RGCs, we followed a previously developed immunohistochemistry (IHC) based method described and validated (4, 5, 17). Further details are provided in *SI Materials and Methods*.

For quantification of excitatory synapse number in mouse brain, three sagittal brain sections per animal were stained with pre- and postsynaptic markers, and 5-μm confocal scans were performed (optical section width, 0.38 μm; 15 optical sections each) at the superficial layer of the SC (five optical sections per section, 15 images per brain). Average synaptic density per imaged area was calculated for each condition. Details on IHC conditions, image acquisition, and quantification can be found in *SI Materials and Methods*.

Electrophysiology. Miniature excitatory postsynaptic currents (mEPSCs) were recorded by whole-cell patch clamping RGCs at room temperature (18 °C–22 °C) at a holding potential of −70 mV. The extracellular solution contained (in mM) 140 NaCl, 2.5 $CaCl_2$, 2 $MgCl_2$, 2.5 KCl, 10 glucose, 1 NaH_2PO_4, and 10 Hepes (pH 7.4), plus TTX (1 μM) to isolate mEPSCs. Patch pipettes were 3 to 5 MΩ and the internal solution contained (in mM) 120 K-gluconate, 10 KCl, 10 EGTA, and 10 Hepes (pH 7.2). mEPSCs were recorded using pClamp software for Windows (Axon Instruments), and were analyzed with Mini Analysis Program (SynaptoSoft).

EM. RGCs were fixed for EM in 4% glutaraldehyde in PBS solution as previously described (4, 6) and viewed with a Philips Electronic Instruments CM-12 transmission electron microscope. Synapses were counted by eye under the electron microscope by finding a cell body and dendrites and counting all synapses within a circular field of radius approximately one cell body-diameter.

SCs from three P25 hevin-null mice on a 129/Sve background and three age-matched WT controls were prepared for EM analysis. Sections at 50 nm were viewed under a Philips Electronic Instruments CM-12 transmission electron microscope. Individual neuronal cell bodies were picked within the

area of 50 to 150 μm under the pia corresponding to the target zone of RGCs. High-magnification (13,000×) consecutive images were taken in a diameter of 20 μm around the cell body. These images were then tiled together by using the Photomerge algorithm in Photoshop software package (Adobe). Synapses were counted blind to the genotype, and their morphological parameters were analyzed by hand using ImageJ software (NIH).

IHC and Western Blotting. For hevin immunostaining, rat anti-hevin monoclonal antibody 12:155 was used (1 μg/mL). For SPARC and nestin stainings, SPARC polyclonal antibody (1 μg/mL; R&D Systems), and rabbit anti-nestin (1:1,000; Covance) were used. Secondary Alexa-conjugated antibodies (Invitrogen) were used at 1:200 dilution for detection. Slides were mounted in Vectashield with DAPI and were imaged on a Leica SP5 confocal laser-scanning microscope.

For Western blot analysis of hevin and SPARC levels in WT mice of different ages, SCs were dissected from four or five mice per age. Protein lysate (15 μg) was loaded into each well. Hevin was detected in Western blots by the rat monoclonal antibody 12:155 or by goat anti-hevin polyclonal antibodies (0.1 μg/mL; R&D Systems). SPARC was detected in the Western blots by goat anti-SPARC polyclonal antibodies (0.1 μg/mL; R&D Systems). Horseradish peroxidase conjugated anti-rat or anti-goat (1:5,000) IgGs were used as secondary antibodies (Jackson Labs), and the detection was performed with an ECL kit (GE) or SuperSignal West Femto detection kit (Pierce). Further details can be found in *SI Materials and Methods*.

Golgi–Cox Staining and Dendritic Morphology Analysis. Golgi–Cox staining was performed on hevin-null and age-matched WT control mice (three mice per genotype) as described in the FD Rapid GolgiStain Kit (FD NeuroTechnologies). RGC target neurons in the SC, the wide-field vertical type-II ganglion cells (WFII), and stellate neurons (26, 27) were analyzed for their morphology (three brains per genotype, $n = 22$ neurons total per cell type) with the Neurolucida tracing tool (MBF Bioscience). The dendritic trees of each neuron were determined for area and perimeter by convex hull analysis, and the complexity of the dendritic tree was calculated by Sholl analysis. All analyses were performed using NeuroExplorer (MBF Bioscience). Further details on staining and morphology analysis are provided in *SI Materials and Methods*.

ACKNOWLEDGMENTS. We thank Maria L. Fabian for excellent technical assistance. This work was supported by National Institute of Drug Addiction Grant DA15043 (to B.A.B.) and National Institutes of Health Grant GM40711 (to E.H.S.). C.E. and N.J.A. were supported by Human Frontiers Scientific Program long-term fellowships. C.E. is a Klingenstein Award Fellow and an Alfred A. Sloan Foundation Fellow.

1. Bolton MM, Eroglu C (2009) Look who is weaving the neural web: Glial control of synapse formation. *Curr Opin Neurobiol* 19:491–497.
2. Eroglu C, Barres BA (2010) Regulation of synaptic connectivity by glia. *Nature* 468: 223–231.
3. Meyer-Franke A, Kaplan MR, Pfrieger FW, Barres BA (1995) Characterization of the signaling interactions that promote the survival and growth of developing retinal ganglion cells in culture. *Neuron* 15:805–819.
4. Christopherson KS, et al. (2005) Thrombospondins are astrocyte-secreted proteins that promote CNS synaptogenesis. *Cell* 120:421–433.
5. Eroglu C, et al. (2009) Gabapentin receptor alpha2delta-1 is a neuronal thrombospondin receptor responsible for excitatory CNS synaptogenesis. *Cell* 139: 380–392.
6. Ullian EM, Sapperstein SK, Christopherson KS, Barres BA (2001) Control of synapse number by glia. *Science* 291:657–661.
7. Liauw J, et al. (2008) Thrombospondins 1 and 2 are necessary for synaptic plasticity and functional recovery after stroke. *J Cereb Blood Flow Metab* 28:1722–1732.
8. Bornstein P, Sage EH (2002) Matricellular proteins: Extracellular modulators of cell function. *Curr Opin Cell Biol* 14:608–616.
9. Cahoy JD, et al. (2008) A transcriptome database for astrocytes, neurons, and oligodendrocytes: A new resource for understanding brain development and function. *J Neurosci* 28:264–278.
10. Eroglu C (2009) The role of astrocyte-secreted matricellular proteins in central nervous system development and function. *J Cell Commun Signal* 3:167–176.
11. Brekken RA, Sage EH (2001) SPARC, a matricellular protein: At the crossroads of cell-matrix communication. *Matrix Biol* 19:816–827.
12. Johnston IG, Paladino T, Gurd JW, Brown IR (1990) Molecular cloning of SC1: A putative brain extracellular matrix glycoprotein showing partial similarity to osteonectin/BM40/SPARC. *Neuron* 4:165–176.
13. Lively S, Ringuette MJ, Brown IR (2007) Localization of the extracellular matrix protein SC1 to synapses in the adult rat brain. *Neurochem Res* 32:65–71.
14. McKinnon PJ, Margolskee RF (1996) SC1: A marker for astrocytes in the adult rodent brain is upregulated during reactive astrocytosis. *Brain Res* 709:27–36.
15. Mendis DB, Brown IR (1994) Expression of the gene encoding the extracellular matrix glycoprotein SPARC in the developing and adult mouse brain. *Brain Res Mol Brain Res* 24:11–19.
16. Mendis DB, Ivy GO, Brown IR (1996) SC1, a brain extracellular matrix glycoprotein related to SPARC and follistatin, is expressed by rat cerebellar astrocytes following injury and during development. *Brain Res* 730:95–106.
17. Ippolito DM, Eroglu C (2010) Quantifying synapses: An immunocytochemistry-based assay to quantify synapse number. *J Vis Exp* 45:pii2270.
18. Mendis DB, Malaval L, Brown IR (1995) SPARC, an extracellular matrix glycoprotein containing the follistatin module, is expressed by astrocytes in synaptic enriched regions of the adult brain. *Brain Res* 676:69–79.
19. Vincent AJ, Lau PW, Roskams AJ (2008) SPARC is expressed by macroglia and microglia in the developing and mature nervous system. *Dev Dyn* 237:1449–1462.
20. Webersinke G, Bauer H, Amberger A, Zach O, Bauer HC (1992) Comparison of gene expression of extracellular matrix molecules in brain microvascular endothelial cells and astrocytes. *Biochem Biophys Res Commun* 189:877–884.
21. Au E, et al. (2007) SPARC from olfactory ensheathing cells stimulates Schwann cells to promote neurite outgrowth and enhances spinal cord repair. *J Neurosci* 27: 7208–7221.
22. Bampton ET, Ma CH, Tolkovsky AM, Taylor JS (2005) Osteonectin is a Schwann cell-secreted factor that promotes retinal ganglion cell survival and process outgrowth. *Eur J Neurosci* 21:2611–2623.
23. Sullivan MM, Sage EH (2004) Hevin/SC1, a matricellular glycoprotein and potential tumor-suppressor of the SPARC/BM-40/Osteonectin family. *Int J Biochem Cell Biol* 36: 991–996.
24. Lund RD, Lund JS (1972) Development of synaptic patterns in the superior colliculus of the rat. *Brain Res* 42:1–20.
25. Sachs GM, Jacobson M, Caviness VS, Jr. (1986) Postnatal changes in arborization patterns of murine retinocollicular axons. *J Comp Neurol* 246:395–408.
26. Ogawa T, Takahashi Y (1981) Retinotectal connections within the superficial layers of the cat's superior colliculus. *Brain Res* 217:1–11.
27. Warton SS, Jones DG (1985) Postnatal development of the superficial layers in the rat superior colliculus: A study with Golgi-Cox and Klüver-Barrera techniques. *Exp Brain Res* 58:490–502.
28. Colonnese MT, Constantine-Paton M (2006) Developmental period for N-methyl-D-aspartate (NMDA) receptor-dependent synapse elimination correlated with visuotopic map refinement. *J Comp Neurol* 494:738–751.
29. Lee PH, Schmidt M, Hall WC (2001) Excitatory and inhibitory circuitry in the superficial gray layer of the superior colliculus. *J Neurosci* 21:8145–8153.
30. Jones EV, et al. (2011) Astrocytes control glutamate receptor levels at developing synapses through SPARC-beta-integrin interactions. *J Neurosci* 31:4154–4165.
31. Aghajanian GK, Bloom FE (1967) The formation of synaptic junctions in developing rat brain: A quantitative electron microscopic study. *Brain Res* 6:716–727.
32. Nie J, et al. (2008) IFATS collection: Combinatorial peptides identify alpha5beta1 integrin as a receptor for the matricellular protein SPARC on adipose stromal cells. *Stem Cells* 26:2735–2745.
33. Weaver MS, Workman G, Sage EH (2008) The copper binding domain of SPARC mediates cell survival in vitro via interaction with integrin beta1 and activation of integrin-linked kinase. *J Biol Chem* 283:22826–22837.
34. Chandrasekaran V, Ambati J, Ambati BK, Taylor EW (2007) Molecular docking and analysis of interactions between vascular endothelial growth factor (VEGF) and SPARC protein. *J Mol Graph Model* 26:775–782.
35. Kelly KA, et al. (2007) SPARC is a VCAM-1 counter-ligand that mediates leukocyte transmigration. *J Leukoc Biol* 81:748–756.
36. Bradshaw AD (2009) The role of SPARC in extracellular matrix assembly. *J Cell Commun Signal* 3:239–246.
37. Weaver MS, et al. (2010) Processing of the matricellular protein hevin in mouse brain is dependent on ADAMTS4. *J Biol Chem* 285:5868–5877.
38. Lu W, Constantine-Paton M (2004) Eye opening rapidly induces synaptic potentiation and refinement. *Neuron* 43:237–249.
39. Vialou V, et al. (2010) DeltaFosB in brain reward circuits mediates resilience to stress and antidepressant responses. *Nat Neurosci* 13:745–752.
40. Mendis DB, Ivy GO, Brown IR (2000) Induction of SC1 mRNA encoding a brain extracellular matrix glycoprotein related to SPARC following lesioning of the adult rat forebrain. *Neurochem Res* 25:1637–1644.
41. Menon PM, Gutierrez JA, Rempel SA (2000) A study of SPARC and vitronectin localization and expression in pediatric and adult gliomas: high SPARC secretion correlates with decreased migration on vitronectin. *Int J Oncol* 17:683–693.
42. Schultz C, Lemke N, Ge S, Golembieski WA, Rempel SA (2002) Secreted protein acidic and rich in cysteine promotes glioma invasion and delays tumor growth in vivo. *Cancer Res* 62:6270–6277.
43. Sage EH (2003) Purification of SPARC/osteonectin. *Curr Protoc Cell Biol* 10:11.1–11.23.